Affinity of Glycan-Modified Nanodiamonds towards Lectins and Uropathogenic Escherichia Coli

Volodymyr Turcheniuk, Kostiantyn Turcheniuk, Julie Bouckaert, Alexandre Barras, Tetiana Dumych, Rostyslav Bilyy, Vladimir Zaitsev, Aloysius Siriwardena, Qi Wang, Rabah Boukherroub, et al.

Post-print

Affinity of Glycan-Modified Nanodiamonds towards Lectins and Uropathogenic *Escherichia Coli*

Authors:

Volodymyr Turcheniuk, Dr Kostiantyn Turcheniuk, Dr Julie Bouckaert, Alexandre Barras, Dr Tetiana Dumych, Dr Rostyslav Bilyy, Prof. Vladimir Zaitsev, Dr. Aloysius Siriwardena, Dr. Qi Wang, Dr. Rabah Boukherroub, and Prof. Sabine Szunerits

First published: 24 February 2016

DOI: 10.1002/cnma.201500229

Abstract. Nanodiamond particles (NDs) modified with glycan ligands are revealing themselves to have great promise as new nanomaterials for combating biofilm formation and as promising anti-adhesive scaffolds. Currently, the strategies at hand to formulate glycan-modified NDs (glyco-NDs) are limited to a few reports. We demonstrate herein that the photoinduced covalent attachment of unmodified sugars results in glyco-NDs with high binding affinity to lectins and a uropathogenic *Escherichia coli* strain (*E. coli* UTI89). While the binding affinities of glyco-NDs to different lectins is partially sacrificed when monosaccharides such as mannose are photochemically integrated onto NDs, in the case of disaccharides and oligosaccharides the binding affinity of glyco-NDs to lectins is preserved. Moreover, mannan-modified NDs show strong interactions with uropathogenic *E. coli*., suggesting the effectiveness of photochemically formed glyco-NDs for disruption of *E. coli*-mediated biofilms.

1. Introduction

The design and preparation of sugar-coated nanoparticles and their applications as polyvalent tools to study and intervene in carbohydrate-mediated interactions have received sustained attention over the past years.[1-6] Carbohydrates are very important components of living organisms and have been identified to play a central role in a large panel of biological processes such as cell–cell communication, viral and bacterial infection, and inflammation and immune responses. The extremely low affinity of carbohydrates, typically in the milli- to micromolar range [mm–μm],[7] to biological objects is compensated for by nature using clustering effects resulting in higher affinities towards the glycan targets. This cooperative multivalent interaction is significantly stronger than the corresponding monovalent one, resulting in nanomolar [nM] affinities and high selectivities. Next to the design of high-affinity glycan ligands,[3, 8-10] the integration of carbohydrates onto nanometric scaffolds has become a well-accepted strategy to mimic glycan-clustering effects of nature and to provide a surface with multivalent carbohydrate presentation.

One of the first types of multivalent nanoscaffolds developed and used as an adhesion inhibitor is gold glycoconjugates.[3, 11] Next to gold, carbon-based nanomaterials have been investigated as glycan scaffolds as they comply well with several requirements needed such as easy and stable surface functionalization, good dispersibility in aqueous media, and broad availability.[1, 4, 6, 8, 12, 13] Next to fullerene-based glycoclusters,[8, 13, 14] nanodiamonds (NDs) are emerging as particularly well-suited for multivalent applications.[1, 4, 6, 12, 15] Amongst the advantages of NDs over other carbon-based materials is that they are completely inert, optically transparent, biocompatible, have the ability to emit light, and can be functionalized in many ways depending on their intended ultimate application.[16-21] Although in vivo toxicity of nanoparticles is dependent on specific *surface characteristics*, ND particles did not induce significant cytotoxicity in a variety of cell lines[22, 23] and were used in various biomedical applications.[24-26]

Despite their evident potential for glycobiology, there are only few reports on glyco-nanodiamonds (glyco-NDs).[1, 4, 6, 12] Krueger and co-workers used a multistep reaction including a Diels–Alder cycloaddition of 1,2-dimethylbromide phenol to the ND surface, followed by a classical aromatic sulfonation and reduction to thiol.[4] The thiol-modified NDs were used as anchors for allyl-modified glycans in a "thiol-ene" type reaction and allowed the efficient detection and removal of pathogenic bacteria. More recently, they have shown the potential of thiourea-bridged ND glycoconjugates to inhibit bacterial adhesion.[6] We have constructed glyco-NDs through the covalent conjugation of propargyl-terminated sugar components to azide-functionalized NDs, as well as the conjugation of azide-terminated sugars to propargyl-terminated NDs.[1, 27] It was demonstrated that these glyco-NDs inhibit type 1 fimbriae-mediated yeast-agglutination and human bladder-cell adherence in a sugar-selective manner. The eukaryotic cell-adherence inhibitory efficiency of ND-mannose was revealed to be far superior to those reported for other glycan-modified particles and nanostructures directed against *E. coli*.

Yet, the requirement for prior derivatization of the appropriate glycan presents a significant hurdle for the construction of glyco-NDs, as the synthetic effort increases exponentially from mono- to di- and oligosaccharides. A recently developed strategy for the formation of gold glyconanoparticles involved photoinduced covalent attachment of native carbohydrates.[28, 29] The method takes advantage of the photochemistry of arylazides, which upon light activation convert to reactive nitrenes.[30] The highly reactive nitrene intermediate formed is believed to interact with glycans through C−H and N−H insertion reactions, creating highly robust covalent linkages. We recently compared the effectiveness of mannose-modified surfaces either formed photochemically or via Cu^{I} "click" reactions for lectin recognition using surface plasmon resonance.[31] Although photochemical surface conjugation did not give anomeric center-specific surface attachment, this was seen not to have a bearing on lectin recognition, with preserved binding affinity and specificity.

The purpose of this work is to make the photochemical strategy available for the formation of a variety of glyco-NDs. Certainly, one drawback of the proposed photochemical approach is the nonspecificity of the coupling reaction, where the attachment of glycans to NDs does not occur exclusively via their reducing ends. It will be shown that the binding affinities of glyco-NDs to lectins is partially sacrificed when monosaccharides such as mannose are linked, while with disaccharides and oligosaccharides the binding affinity of glyco-NDs to lectins is entirely preserved.

DOI: 10.1002/cnma.201500229 – Journal: ChemNanoMa– Post-print

In addition, we examined whether these glyco-NDs show affinity to a uropathogenic *Escherichia coli* strain (*E. coli* UTI89). Among the targets that have been identified for the development of anti-adhesive strategies are type-1 fimbriae, which constitute major virulence factors produced by *E. coli* UTI89.[32] Type-1 fimbriae are filamentous tubular structures each of 0.2–2.0 μm in length and 5–7 nm in diameter that are distributed over the entire surface of the bacterium. The lectin located at the extremity of type-1 fimbriae, FimH, contributes to tissue colonization through its specific recognition of the terminal α-d-mannopyranosyl units present on cell-surface glycoproteins. We have recently demonstrated that mannose-modified NDs exhibit marked anti-adhesive activity for *E. coli* UTI89 in cell-based assays without displaying toxicity against eukaryotic cells.[1, 12] The coupling strategy used for the fabrication of these particles was based on the Cu^{I}-catalyzed Huisgen cycloaddition reaction (“click” reaction) between NDs decorated with surface azidophenyl or propargyl functions and the corresponding synthetic sugar analogue. Herein, we investigate the potential of photochemically grafted native mannose versus mannan to interact with *E. coli* UTI89 using a fluorescence-based agglutination assay.[33]

2. Results and discussion

2.1. Synthesis of glyco-NDs via photoactivation of perfluorophenylazide-modified NDs

We have recently shown that dopamine, known to have strong interactions with different metal oxides and graphene-like structures, is a viable agent for the functionalization of nanodiamonds.[16, 27] A dopamine derivative of perfluorophenylazide (**1**) was therefore synthesized through reaction of the *N*-succinimidyl 4-azidotetrafluorobenzoate with the amine groups of dopamine (Figure 1 A). Hydroxylated nanodiamonds (ND-OH) were subsequently functionalized with ligand (**1**) (Figure 1 B). The functionalized ND particles (ND-PFPA) were characterized by Fourier transform infrared (FTIR) spectroscopy (Figure 2 A) and X-ray photoelectron spectroscopy (XPS) (Figure 2 B).

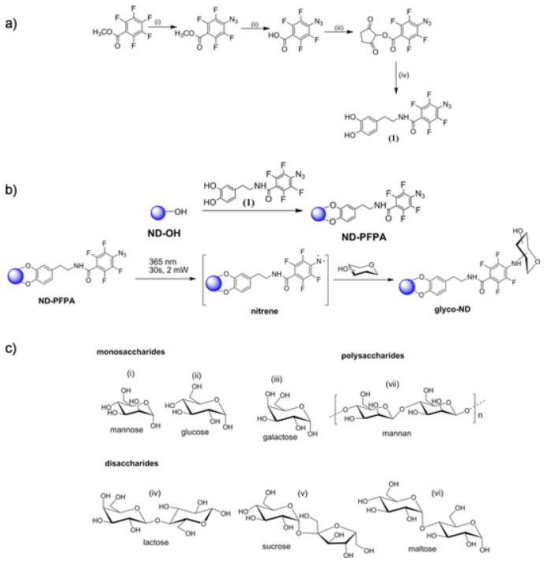

Figure 1.

DOI: 10.1002/cnma.201500229 – Journal: ChemNanoMa– Post-print

a) Synthesis of perfluorophenyl azide (PFPA)-modified dopamine (**1**): (i) NaN_3, acetone/water, 90 °C, 2 h, 85 %; (ii) NaOH, water, 3 h, RT, 90 %, (iii) NHS, DCM, RT, overnight; 95 %, (iv) dopamine hydrochloride, TEA, DMF, RT, argon, 91.4 %. b) Modification of ND-OH with ligand (**1**) forming ND-PFPA. c) Formation of glyco-NDs through the photochemical linking of mono-, di-, and a polysaccharide onto NDs.

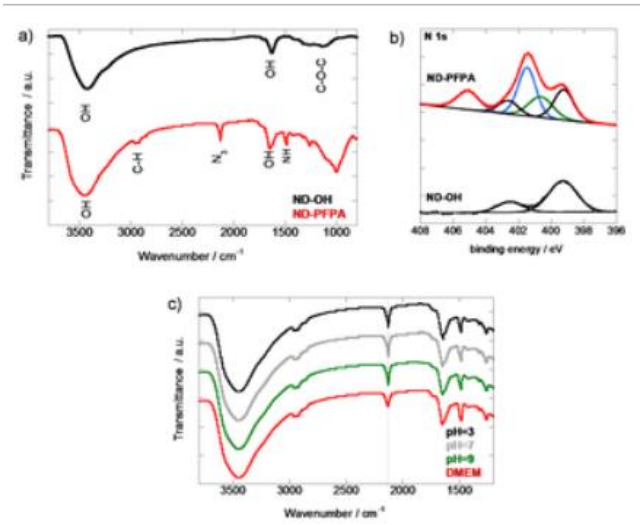

Figure 2.

a) FTIR spectra of ND-OH (black) and ND-PFPA (red). b) N 1s high-resolution XPS spectra of ND-OH (black) and ND-PFPA (red). c) FTIR spectra of ND-PFPA after immersion for 24 h in pH 3, pH 7, pH 9, and DMEM.

The FTIR spectrum of the as-received ND-OH (Figure 2 A) shows a broad peak at 3447 cm^{-1} assigned to the vibration of surface hydroxyl groups or/and adsorbed water molecules, and an additional sharper one at 1633 cm^{-1} due to the bending mode $\delta_{(OH)}$ of surface hydroxyl groups on the NDs. In addition, the band at 1107 cm^{-1} is indicative of the presence of C−O−C− functional groups of cyclic ethers. After reaction of ND-OH particles with ligand (**1**) a new vibration peak at 2125 cm^{-1} characteristic of the $\nu_{as(N3)}$ stretching appears. The C−H stretching vibration modes are detected at 2850–2970 cm^{-1} and are partially masked by the large band at 3447 cm^{-1}. The ND-PFPA particles display in addition a band at 2125 cm^{-1} characteristic of the $\nu_{as(N3)}$ stretching mode and a band at 2936 cm^{-1} characteristic of the presence of C−H bonds, as reported previously.[16] The band at 1546 cm^{-1} is most likely associated with the −NH−C=O bond present in ligand (**1**).

The presence of the azide group on ND-PFPA is in addition confirmed by the N 1s high resolution XPS spectrum (Figure 2 B). Bands at 405.2 (Ar−N=N^+=N^-) and 401.9 eV (Ar−N=N^+=N^-), characteristic for the $-N_3$ groups, are observed. The contribution of the −NH−C=O linkage is seen at 400.6 eV. Bands at 402.7 and 399.2 eV are also observed in the initial ND−OH. These correspond most likely to nitrogen functions such as N−O and C−N most likely generated during the detonation process of trinitrotoluene with formation of NDs. As seen in Table 1, the nitrogen content accounts for 1.5 at % and might be responsible for the

DOI: 10.1002/cnma.201500229 – Journal: ChemNanoMa– Post-print

positive surface potential of ND-OH (Table 1), as also reported by others. The level of N 1s is increased in ND-PFPA particles to 8.4 at % with a F/(N-1.5) ratio of 1.28, close to the theoretical value of 1.33.

Table 1. Physical properties of the NDs modified with ligands (1).

NDs	Diameter [nm]	PDI[a]	Zeta potential [mV]	N[b] [%]	F[b] [%]
ND-OH	79±13	0.246±0.002	35±2	1.5	0.0
ND-PFPA	126±3	0.168±0.021	34±2	8.4	6.9

[a] Polydispersity index. [b] Atomic percent according to XPS survey spectrum.

To ensure the stability of the conjugates and that the dopamine ligand does not detach over time, ND-PFPA particles were immersed for 24 h at different pH (3, 7, and 9) as well as in biological medium such as Dulbecco′s modified Eagle medium (DMEM) and the FTIR spectra were recorded. As seen from Figure 2 C, no significant decrease of the $\nu_{as(N3)}$ band at 2125 cm^{-1} is observed upon immersion into solutions of different pH, and only a slight decrease was observed when incubated in biological medium. The ether bond between the diamond surface and the aromatic ring of dopamine seems to be rather stable and comparable of those on organic molecules with no hydrolysis taking place at this timeframe.

Photochemical linkage of glycans to NDs takes advantage of the photochemistry of arylazides, which upon light activation convert to reactive nitrenes (Figure 1 C). The highly reactive nitrenes can interact directly with any glycan through C−H and/or N−H insertion reactions, creating highly robust covalent linkage. Mono-, di- and a polysaccharide were photochemically integrated onto ND-PFPA particles (Figure 1 C) by mixing a solution of ND-PFPA in acetonitrile with aqueous solutions of the respective glycan, and irradiating the mixtures at 365 nm for 30 s at 2 mW. Representative FTIR spectrum of mannose and mannan-modified NDs are shown in Figure 3 B and show the complete disappearance of the characteristic −N3 vibration band at 2128 cm−1, suggesting that all the azido groups were consumed in the photochemical process. The band at 1633 cm−1 due to the bending mode δ(OH) increased significantly in the case of ND-mannan. The N 1s XPS spectra after photochemical linking of mannose also changed significantly. The conversion of the azide group into C−N bonds is evidenced by the disappearance of the bands at 405.2 (Ar−N=N+=N−) and 401.9 eV (Ar−N=N+=N−) and the appearance of a band at 400.6 eV due to the formation of C−N bonds. The presence of F 1s signal at 686 eV is an additional indication of the formation of ND-mannose (Figure 3 C). To validate further the covalent linking of the glycan to ND-PFDA, a solution of ND-PFPA in acetonitrile was mixed with an aqueous solution of mannan and left for 24 h. The characteristic −N3 vibration band at 2128 cm−1 was still present on ND-PFPA confirming the interaction of the glycan with the dopamine ligand on the NDs.

DOI: 10.1002/cnma.201500229 – Journal: ChemNanoMa– Post-print

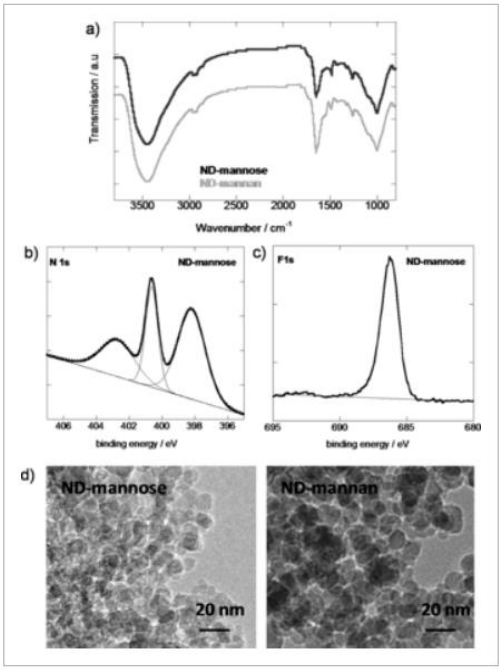

Figure 3.

a) FTIR spectra of ND-mannose (black) and ND-mannan (grey); b) N 1s spectrum of ND-mannose; c) F 1s spectrum of ND-mannose; d) TEM images of ND-mannose and ND-mannan.

Representative transmission electron microscopy (TEM) images of ND-mannose and ND-mannan (Figure 3 D) reveal the presence of spherical particles with a mean diameter of 24±8 nm for all structures independent of the glycan present on their surface.

The amount of glycan integrated onto ND-PFPA was analyzed using the well-established phenol–sulfuric acid assay and proved to be glycan dependent (Table 2). In the case of mannose, the sugar loading is comparable to mannose-ND formed via “click” chemistry as reported previously by us.[1] In the case of disaccharide-modified NDs, the amount of incorporated saccharides is about twice that of mannose, with the highest sugar loading observed for mannan-NDs.

Table 2. Physical properties of different glycan-NDs.

DOI: 10.1002/cnma.201500229 – Journal: ChemNanoMa– Post-print

Materials	Diameter [nm]	PDI[a]	Zeta potential [mV]	Sugar loading [μg mg^{-1} ND]
mannose-NDs	127±7	0.190±0.020	32±2	95±9
glucose-NDs	104±3	0.163±0.031	28±2	89±7
galactose-NDs	113±3	0.145±0.026	30±2	96±10
lactose-NDs	97±3	0.148±0.030	31±2	110±12
sucrose-NDs	105±3	0.159±0.026	25±2	138±15
maltose-NDs	98±3	0.167±0.024	25±2	120±15
mannan-NDs	101±3	0.187±0.025	17±2	315±20

[a] Polydispersity index.

2.2 Lectin binding assays

The glyco-NDs were subjected to affinity binding studies with a series of fluorescently labeled lectins (Figure 4). FITC-labeled *Concanavalin A* from *Canavalia ensiformis* (Con A) and FTIR-labeled *Lens culinaris (*LENS*)* are primarily selective towards to mannopyranoside and were used as positive controls. The α-d-galactopyranose specific *Arachis hypogaea* (PNA) was used as negative control for mannose-, glucose-, sucrose-, maltose-, and mannan-modified ND particles, while Con A and LENS were negative controls for galactose-modified NDs. Lactose-NDs are expected to interact with all lectins as this disaccharide is derived from the condensation of galactose and glucose-forming β(1→4)glycosidic linkage. The fluorescence intensities recorded after interaction of glyco-NDs solutions for 30 min with different lectins confirm that the binding affinities of the photolinked sugars are in accordance with the expected binding characteristics for each lectin. Mannose-modified NDs exhibit several times larger fluorescence signals when incubated with Con A and LENS than with PNA due to the higher binding affinity. The fluorescence intensity recorded for mannose-NDs in the presence of FITC-labeled PNA is of the same magnitude than that measured using ND−OH. This fluorescence level is thus most likely linked to nonspecific interaction of the protein with the particle surface. Galactose-modified NDs show the opposite behavior, strong fluorescence upon incubation with PNA and weak with Con A and LENS lectins. In the case of glucose-NDs, the fluorescence signal upon incubation is strongest for LENS, lower for Con A, and weak for PNA. The tetrameric lectin Con A has next to mannose a reported binding site specific to glucose, with however a lesser extent. The lowered fluorescence signal upon incubation of glucose-ND with Con A when compared to glucose-ND specific LENS correlates to this difference in affinity.

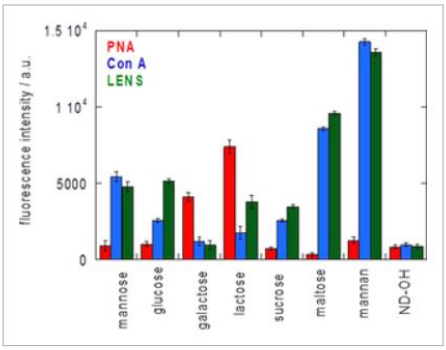

Figure 4.

DOI: 10.1002/cnma.201500229 – Journal: ChemNanoMa– Post-print

Fluorescence intensities evaluated using FTIC-labeled lectins after reaction with glycan-terminated NDs in a 1/1 ratio (1 mg mL^{-1}) in tris buffer solution (pH 7.4 containing Mg^{2+}, Ca^{2+}, NaCl): Fluorescent measurements were performed using an excitation wavelength of 485 nm and an emission wavelength of 520 nm; the results are derived from the data of 4 independent experiments.

To further investigate the generality of this coupling method and the specificity to surface-bound glycans, disaccharide, polysaccharide, and mannan were each photochemically linked to ND-PFPA and their affinity towards the three lectins was determined. The interaction of lactose-NDs with PNA or LENS resulted in about twice the fluorescence signal for PNA. This disaccharide seems to be preferentially coupled to the NDs via its glucose end. In the case of sucrose-NDS, a disaccharide composed of glucose and fructose, no interaction with PNA was observed, while the interaction with glucose-specific Con A and LENS was higher, suggesting that some of the sucrose is linked via the fructose end to ND-PFPA. Using maltose-ND, a disaccharide formed from two units of glucose with an α(1→4) bond, strong binding to Con A and LENS were observed, being stronger than that obtained with mannose.

The strongest interaction with Con A and LENS is observed with mannan-modified NDs. These particles showed a three times higher sugar loading than mannose-NDs, which correlates to an approximately three times larger fluorescent signal.

2.3 Effect of mannose-NDs and mannan-NDs on agglutination of *E. coli* UTI89 strains

Fluorescence-based agglutination assay in the presence of mannose and mannose-NDs

Next, we examined whether mannose-NDs and mannan-NDs show affinity to uropathogenic *E. coli* UTI89. As discussed in the introduction, FimH, a lectin located at the extremity of type 1 fimbriae, is a major virulence factor produced by *E. coli* UTI89, and contributes to tissue colonization through its specific recognition of the terminal α-d-mannopyranosyl units present on cell-surface glycoproteins. Interfering with this interaction has been recently shown to be possible with mannose-modified NDs formed by "click" chemistry of propargyl and/or azide-modified mannose derivatives.[1, 12] To scrutinize the potential of the photochemically formed mannose-NDs, we investigated if such particles display enhanced agglutination effects towards *E. coli* UTI89 when compared to free mannose in solution. A fluorescence-based agglutination assay was used for this purpose.[33] It is based on mixing different concentrations of mannose and mannose-NDs with fluorescently labeled *E. coli* UTI89 formed through genetic modification to express turboFP635 (Katushka) fluorescent proteins, emitting at 635 nm (upon excitation at 580 nm).[34] Figure 5 depicts diverse fluorescence images of Katushka expressing *E. coli* after interaction for 4 h at 4 °C with different concentrations of mannose-NDs (1–300 μg mL^{-1}). As a control, the influence of ND-OH and mannose in solution were investigated. These agglutination tests show that mannose, as expected, gives no *E. coli UTI89* agglutination in the concentration range tested. In contrast to free mannose in solution, mannose-NDs display a concentration dependent agglutination behavior at a minimal concentration of ≈50 μg mL^{-1}.

DOI: 10.1002/cnma.201500229 – Journal: ChemNanoMa– Post-print

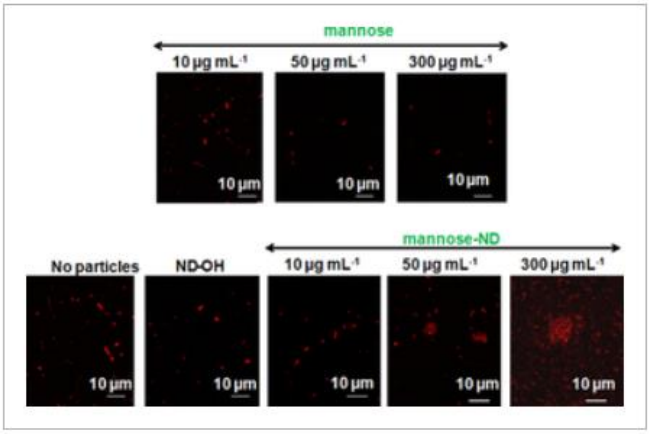

Figure 5.

Fluorescence-based agglutination assay for: Fluorescence images of Turbo FP635 (Katushka protein) expressing *E. coli* UTI89 (1×10^8 cfu ml^{-1}) in the presence of different concentrations of mannose, in the absence of particles (no particles) and in the presence of ND-OH (100 µg mL^{-1}) and different mannose-NDs (the values correspond to total mannose concentration in the solution and is directly comparable with the results of free mannose).

Fluorescence-based agglutination assay in the presence of mannan and mannan-NDs

In addition, the agglutination behavior of mannan and mannan-NDs was investigated in a comparable manner. Mannan is a cell-wall component of microorganisms, consisting of d-mannose residues expanded by α-(1→6)-, α-(1→3)-, α-(1→2)- linkages. Park and co-workers reported on the formation of carboxylic mannan-coated iron oxide nanoparticles to target antigen-presenting cells (APCs), including macrophages, by the specific interaction between the mannose ligand and the mannose receptors on APCs.[35] The choice of mannan as the integral component in NDs is to take advantage of the expected high binding affinity towards *E. coli* UTI89 due to the presence of multiple mannose ligands in this polysaccharide. Figure 6 exhibits the results of mannan and mannan-NDs addition to a solution of *E. coli* UTI89. In contrast to mannose only (Figure 5), addition of 100 µg mL^{-1} mannan reveals partial *E. coli* UTI89 agglutination. Moreover, mannan-ND particles have an ability to agglutinate *E. coli* with an onset at concentrations as low as ≈10 µg mL^{-1}. This is in line with the believed multivalent presentation of mannan on nanoparticles.

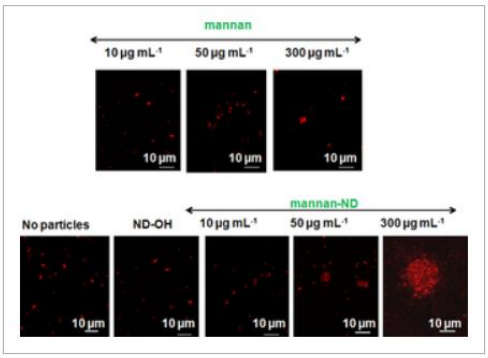

DOI: 10.1002/cnma.201500229 – Journal: ChemNanoMa– Post-print

Figure 6.

Fluorescence-based agglutination assay for: Fluorescence images of Turbo FP635 (Katushka protein) expressing *E. coli* UTI89 (1×10^8 cfu ml^{-1}) in the presence of different concentrations of mannan, in the absence of particles (no particles) and in the presence of ND-OH (100 μg mL^{-1}) and different mannan-NDs (the values correspond to total mannan concentration in the solution and is directly comparable with the results of free mannan).

3. Conclusions

In conclusion, we have shown that photochemical linking of unmodified mono-, di-, and polysaccharides to nanodiamond particles pre-modified with perfluorophenylazide ligands is a general method for coupling underivatized carbohydrates to diamond nanostructures. The coupling method, based on photochemically induced CH insertion is fast and gives a high coupling yield. More importantly, the resulting glyco-NDs maintained their expected binding affinity and specificity towards their partner lectins. These results confirm previous reports on the effectiveness of photochemically formed glycan surfaces to selectively interact with specific lectins. The generality of photochemical approach to provide glyco-NDS was in addition demonstrated through the formation of various disaccharide and a polysaccharide modified NDs. It should be noted, however, that in the case of disaccharide-modified NDS, lactose preferentially couples via the glucose end to NDs, while in the case of sucrose, the fructose end preferential bind photochemically. The reasons for this behavior are currently not understood. "Click" chemistry approaches show a higher degree of control for anchoring disaccharides onto particles. However, this limitation is absent in polysaccharides such as mannan and the approach is believed to be mainly adapted for such glycans. That was the primary motivation for investigating the potential of mannan-NDs to interact with *E. coli* UTI89. Through a fluorescence-based agglutination assay, we showed that mannan-NDs display *E. coli* agglutination at concentrations of ≈10 μg mL^{-1}, which is much lower than that for free mannan and mannose-NDs. Taken together, the findings presented here show that the nanostructures described should be further developed and evaluated as potential anti-adhesives for countering bacterial colonization and infections in vivo.

4 Experimental Section

4.1 Materials

Hydroxyl-terminated nanodiamonds (ND-OH) were purchased from International Technology Center (Raleigh, NC, USA).

All chemicals were of reagent grade or higher and were used as received unless otherwise specified. Methyl pentafluorobenzoate, sodium azide (NaN_3), dimethylformamide (DMF), diethyl ether, magnesium sulfate ($MgSO_4$), acetone, methanol (MeOH), dichloromethane (DCM), sodium hydroxide (NaOH), hydrochloric acid (HCl), *N*,*N*′-dicyclohexylcarbodiimide (DCC), 4-dimethylaminopyridine (DMAP), copper(II) sulfate pentahydrate ($CuSO_4{\cdot}5\,H_2O$), l-ascorbic acid, ethylenediaminetetraacetic acid (EDTA), mannose, glucose, galactose, lactose, sucrose, maltose, mannan (from *Saccharomyces cerevisia*), FITC-labeled *Concanavalin A* (from *Canavalia ensiformis*), FITC-labeled *Lens culinaris* (LENS) and FITC-labeled A*rachis*

DOI: 10.1002/cnma.201500229 – Journal: ChemNanoMa– Post-print

hypogaea (PNA) were obtained from Sigma–Aldrich and used without further purification. Azido benzoic acid was purchased from TCI Europe (Belgium). Ultrapure water (Milli-Q, 18 MΩcm) was used for the preparation of the solutions and for all rinsing steps. Dulbecco′s modified Eagle medium (DMEM) was obtained from Gibco by Life Technologies.

4.2 Synthesis of 4-azido-*N*-(3,4-dihydroxyphenethyl)-2,3,5,6-tetrafluorobenzamide (1)

4.2.1 -Azidotetrafluorobenzoic acid

Pentafluorobenzoic acid methyl ester (PFPA, 300 mg, 1.3 mmol), NaN_3 (129 mg, 2 mmol) were mixed in acetone/water in 2/1 ratio. The mixture was refluxed for 3 h. Afterwards, it was evaporated under reduced pressure and water was added. The precipitate was washed with water several times and dried. Then it was dissolved in 10 % NaOH water/methanol solution and stirred for 4 h, acidified to pH 5 and extracted using CH_2Cl_2. The organic layer was washed with water, dried and evaporated to give 270 mg (86 % yield) of white precipitate. ^{1}H NMR (300 MHz, DMSO): δ=11.3 ppm (1 H). MS (ESI): *m*/*z* (%)=258 $[M+Na]^+$.

N-Succinimidyl 4-azidotetrafluorobenzoate

A solution of 4-azidotetrafluorobenzoic acid (234 mg, 1 mmol), *N*-hydroxysuccinimide (115 mg, 1.00 mmol), and dicyclohexylcarbodiimide (211 mg, 1.02 mmol) in DCM (6.5 mL) was stirred at room temperature overnight. The mixture was filtered. The filtrate was evaporated and the product was purified by column chromatography to give 317.6 mg (95 % yield) as a colorless solid. ^{1}H NMR (300 MHz, DMSO): δ=2.91 ppm (4 H, s). MS (ESI): *m*/*z* (%)=355 $[M+Na]^+$.

4.2.2 -azido-N-(3,4-dihydroxyphenethyl)-2,3,5,6-tetrafluorobenzamide (1)

To a solution of dopamine hydrochloride (113.4 mg, 0.6 mmol) in DMF (4 mL) were added TEA (108.4 mL, 0.77 mmol) and *N*-succinimidyl 4-azidotetrafluorobenzoate (200 mg, 0.6 mmol). The mixture was stirred overnight at room temperature under argon. Then water was added, and the resulting precipitate was filtered and washed with water several times and then dried at 100 °C carefully to give 203 mg (91.4 % yield) of white powder. ^{1}H NMR (300 MHz, DMSO): δ=8.96–8.92 (t, 1 H, amide), 8.80 (s, 1 H, OH), 8.74 (s, 1 H, OH), 6.65–6.13 (m, 2 H, arom) 6.49–6.46 (d, 1 H, arom), 3.42–3.36 (q, 2 H, CH_2NHCO), 2.65–2.60 ppm (t, 2 H, CH_2).

4.3 Formation of ND-PFPA

A suspension of ND-OH particles in anhydrous acetonitrile (10 mg in 5 mL) was added to a solution of ligand (**1**) in acetonitrile (10 mg) and stirred at room temperature for 24 h. The formed ND-PFPA particles were isolated by centrifugation at 10 000 rpm, purified through four consecutive wash/centrifugation cycles at 10 000 rpm with acetonitrile and ethanol, and finally oven dried at 50 °C for 24 h.

4.4 Photochemical linkage of glycans to ND-PFPA

ND-PFPA (in anhydrous acetonitrile (1 mg mL^{-1} in 200 µL) was mixed with an aqueous solution of the respective glycans (Figure 1) (1 mg mL^{-1} in 400 µL) in a quartz cuvette. The

DOI: 10.1002/cnma.201500229 – Journal: ChemNanoMa– Post-print

mixture was irradiated with a UV lamp (Hamamatsu, 2 mW cm^{-2}) for 30 s under vigorous stirring. The resulting glyco-NDs were isolated by centrifugation at 10 000 rpm for 15 min. In order to remove excess mannose, three additional washing/centrifugation cycles at 10 000 rpm with water were performed.

4.5 Determination of carbohydrate loading on the NDs

A calibration curve for carbohydrate concentrations in solution was established. For this, a phenolic aqueous solution (5 wt %, 60 μL) and concentrated H_2SO_4 (900 μL) was added to an aqueous carbohydrate solution (60 μL), stirred for 10 min and then an absorption spectrum of the mixture was recorded (PerkinElmer Lambda 950 dual beam) against a blank sample (without carbohydrate). The absorbance of the solution was measured at two wavelengths: λ_1=495 and λ_2=570 nm and the absorbance difference (A_{495}–A_{570}) was plotted against the concentration of the corresponding carbohydrate. The quantity of surface-linked carbohydrate was determined with 60 μL of the corresponding ND particles solution in water (0.8 mg mL^{-1}), which was treated with phenol/H_2SO_4 following the same protocol described above. ND-OH particles were treated in the same manner and used as a blank sample.

4.6 Lectin binding assay

The binding affinity of the different glycol-NDs was evaluated using FITC-labeled *Concanavalin A* (Con A), FITC-labeled *Arachis hypogaea* (PNA) and FITC-labeled *Lens culinaris* (LENS). The glyco-NDs (1 mg mL^{-1}, 100 μL) suspended in Tris buffer solution (pH 7.4 containing Mg^{2+}, Ca^{2+}, NaCl) were mixed with 300 μL solutions of the different lectins (1 mg mL^{-1}) in Tris buffer solution and the reaction mixture left under gentle shaking for 1 h. In order to remove nonreacted lectins, three additional washing/centrifugation cycles at 10 000 rpm with Tris buffer were carried out. Fluorescent measurements were performed using an excitation wavelength of 485 nm and an emission wavelength of 520 nm (GFP filter).

4.7 Fluorescence-based agglutination assay

To 0.7 mL of *E. coli* UTI89 bacteria (1×10^8 cfu ml^{-1}) expressing the TurboFP635 protein (Katushka) were added 0.3 mL of ND-mannan or ND-mannose particles solution (1 mg mL^{-1}) and kept for 4 h at 4 °C. Thereafter the solutions were dropped onto microscopic slides, covered with cover slips and sealed. Fluorescence images were recorded at an excitation wavelength λ_{ex}=580 nm and an emission wavelength λ_{em}=635 nm.

4.8 Instrumentation

FTIR spectra in transmission mode were recorded using a ThermoScientific FTIR instrument (Nicolet 8700) with a resolution of 4 cm^{-1}. Dried ND powder (1 mg) was mixed with KBr powder (100 mg) in an agate mortar. The mixture was pressed into a pellet under 10 tons load for 2–4 min, and the spectrum was recorded immediately. Sixteen accumulative scans were collected. The signal from a pure KBr pellet was subtracted as a background.

X-ray photoelectron spectroscopy (XPS) experiments were performed in a PHl 5000 VersaProbe - Scanning ESCA Microprobe (ULVAC-PHI, Japan/USA) instrument at a base pressure below 5×10^{-9} mbar. Monochromatic $Al_{K\alpha}$ radiation was used and the X-ray beam, focused to a diameter of 100 μm, was scanned on a 250×250 μm surface, at an operating power

DOI: 10.1002/cnma.201500229 – Journal: ChemNanoMa– Post-print

of 25 W (15 kV). Photoelectron survey spectra were acquired using a hemispherical analyzer at pass energy of 117.4 eV with a 0.4 eV energy step. Core-level spectra were acquired at pass energy of 23.5 eV with a 0.1 eV energy step. All spectra were acquired at 90° between X-ray source and analyzer and with the use of low energy electrons and low energy argon ions for charge neutralization. After subtraction of the Shirley-type background, the core-level spectra were decomposed into their components with mixed Gaussian-Lorentzian (30:70) shape lines using the CasaXPS software. Quantification calculations were performed using sensitivity factors supplied by PHI.

Transmission electron microscopy (TEM) images were recorded on a JEOL JEM-2100 electron microscope operated at an accelerating voltage of 200 kV.

Absorption spectra were recorded using a Jasco V-570 UV/VIS/NIR Spectrophotometer from Jasco Int. Co. Ltd., Tokyo, Japan.

ND suspensions (20 μg mL^{-1}) in water were sonicated. The particle size of the ND suspensions was measured at 25 °C using a Zetasizer Nano ZS (Malvern Instruments S.A., Worcestershire, U.K.) in 173° scattering geometry and the zeta potential was measured using the electrophoretic mode.

Fluorescent measurements were carried out using PHERAstar FS microplate reader using an excitation wavelength of 485 and an emission wavelength of 520 nm.

Confocal fluorescence images were acquired by using a confocal microscope (Leica TCS SP5X, Mannheim, Germany) with a 63× objective (Leica Plan Apo, NA=1.2, water immersion). The photomultiplier tubes integrated to the SP5X were used to detect the fluorescence coming from the turboFP635 (Katushka) fluorescent protein expressed in the bacteria (λ_{ex}=580 nm; λ_{em}=635 nm).

Acknowledgements

Financial support from the Centre National de la Recherche Scientifique (CNRS), the University Lille, the Nord Pas-de-Calais region and the Institut Universitaire de France (IUF) are acknowledged. We also thank the European Union through financial support (FP7-PEOPLE-2010-IRSES) action “Photorelease”, grant number 269009 and H2020-MSCE-RISE-2015 (PANG, Nr. 690836).

References

1. Barras, F. A. Martin, O. Bande, J. S. Baumann, J.-M. Ghigo, R. Boukherroub, C. Beloin, A. Siriwardena, S. Szunerits, *Nanoscale* 2013, 5, 2307.
2. M. Khanal, A. Barras, T. Vausselin, L. Fénéant, R. Boukherroub, A. Siriwardena, J. Dubuisson, S. Szunerits, *Nanoscale* 2015, 7, 1392–1402.
3. M. Marradi, F. Chiodo, I. Garcia, S. Penades, Chem. Soc. Rev. 2013, 42, 4728–4745.
4. M. Hartmann, P. Betz, Y. Sun, S. H. Gorb, T. K. Lindhorst, A. Krueger, *Chem. Eur. J.* 2012, 18, 6485.
5. J. M. Tam, M. K. Mansour, N. S. Khan, N. C. Yoder, J. M. Vyas, *Integr. Biol*. 2012, 4, 220.

DOI: 10.1002/cnma.201500229 – Journal: ChemNanoMa– Post-print

6. Fessele, S. Wachtler, V. Chandrasekaran, C. Stiller, T. K. Lindhorst, A. Kruefer, *Eur. J. Org. Chem*. 2015, 5519–5525.
7. N. Sharon, H. Lis, *Glycobiology* 2004, 14, 53R.
8. S. Cecioni, V. Oerthel, J. Iehl, M. Hoiller, D. Goyard, J.-P. Praly, J. F. Imberty, J.-F. Nierengarten, S. Vidal, *Chem. Eur. J.* 2011, 17, 3252.
9. M. Almant, V. Moreau, J. Kovernsky, J. Bouckaert, S. G. Gouin, *Chem. Eur. J*. 2011, 17, 10029.
10. S. Brument, A. Sivignon, N. Moreau, G. Roos, Y. Gueradel, T. Chalopin, D. Deniaud, R. Bilyy, A. Darfeille-Michaud, J. Bouckaert, S. G. Gouin, *J. Med. Chem*. 2013, 56, 5395–5406.
11. N. C. Reichardt, M. Martin-Lomas, S. Penades, *Chem. Soc. Rev*. 2013, 42, 4358.
12. M. Khanal, F. Larsonneur, V. Raks, A. Barras, J.-S. Baumann, F. A. Martin, R. Boukherroub, J.-M. Ghigo, C. Ortiz Mettet, V. Zaitsev, J. M. Garcia Fernances, C. Beloin, A. Siriwardena, S. Szunerits, *Nanoscale* 2015, 7, 2325–2335.
13. M. Durka, K. Buffet, J. Iehl, M. Holler, D. Hazelard, T. M. Barragan, C. O. Mellet, J.-F. Nierengarten, *Chem. Commun*. 2011, 47, 1321.
14. P. Compain, C. Decroocq, I. Ihel, M. Holler, D. Hazelard, T. M. Barragan, C. O. Mellet, J.-F. Nierengarten, *Angew*. *Chem. Int. Ed*. 2010, 49, 5753.
15. M. Khanal, V. Raks, R. Issa, V. Chernyshenko, A. Barras, J. M. Garcia Fernandes, A. Siriwardena, I. Cooper, P. Cragg, L. I. Mikhalovska, V. Zaitsev, R. Boukherroub, S. Szunerits, *Part. Part. Syst. Charact*. 2015, 32, 822–830.
16. Barras, J. Lyskawa, S. Szunerits, P. Woisel, R. Boukherroub, *Langmuir* 2011, 27, 12451–12457.
17. V. N. Mochalin, O. A. Shenderova, D. Ho, Y. Gogotsi, *Nat. Nanotechnol*. 2012, 7, 11–23.
18. Krueger, Chem. Eur. J. 2008, 14, 1382–1390.
19. J. Slegerova, M. Hajek, I. Rehor, F. Sedlak, J. Stursa, M. Hruby, P. Cigler, *Nanoscale* 2015, 7, 415.
20. L. Zhao, Y.-H. Xu, H. Qin, S. Abe, T. Akasaka, T. Chano, F. Watari, T. Kimura, N. Komatsu, X. Chen, *Adv. Funct. Mater*. 2014, 24, 5348–5357.
21. Rehor, J. Slegerova, J. J. Kucka, V. Proks, V. Petrakova, M.-P. Adam, F. Treussart, S. Turner, S. Bals, P. Sacha, M. Ledvina, A. M. Wen, N. F. Steinmetz, P. Cigler, *Small* 2014, 10, 1106.
22. L. Marcon, F. Riquet, D. Vicogne, S. Szunerits, J. F. Bodart, R. Boukherroub, *J. Mater. Chem.* 2010, 20, 8064–8069.
23. M. Schrand, H. Huang, C. Carlson, J. J. Schlager, E. Osawa, S. M. Hussain, L. Dai, *J. Phys. Chem*. B 2007, 111, 2–7.
24. V. Vaijayanthimala, S. V. Kimb, A. Yen, N. Tsai, D. Ho, H.-C. d. Chang, O. Shenderova, *Expert Opin*. *Drug Delivery* 2015, 12, 735.
25. M. Khanal, T. Vausselin, A. Barras, O. Bande, K. Turcheniuk, M. Benazza, V. Zaitsev, C. M. Teodurescu, R. Boukherroub, A. Siriwardena, J. Dubuisson, S. Szunerits, *ACS Appl. Mater. Interfaces* 2013, 5, 12488–12498.
26. R. Martín, M. Álvaro, J. R. Herance, H. García, *ACS Nano* 2010, 4, 65–74.
27. M. Khanal, V. Turcheniuk, A. Barras, R. Rosay, O. Bande, A. Siriwardena, V. Zaitsev, G.-H. Pan, R. Boukherroub, S. Szunerits, *Langmuir* 2015, 31, 3926–3933.
28. X. Wang, O. Ramstrom, M. Yan, *J. Mater. Chem*. 2009, 19, 8944.
29. X. Wang, E. Matei, L. Deng, O. Ramstrom, M. Gronenborn, M. Yan, *Chem. Commun*. 2011, 47, 8620–8622.
30. X. Wang, O. Ramstrom, M. Yan, *Chem. Commun*. 2011, 47, 4261–4263.

DOI: 10.1002/cnma.201500229 – Journal: ChemNanoMa– Post-print

31. N. Maalouli, A. Barras, A. Siriwardena, R. Boukherroub, S. Szunerits, *Analyst* 2013, 138, 805–812.
32. M. Hartmann, T. K. Linhorst, Eur. J. Org. Chem. 2011, 2011, 3583–3609.
33. X. Yan, A. Sivignon, P. Alcouffe, B. Burdin, S. Favre-Bonté, R. Bilyy, N. Barnich, E. Fleury, E. Ganachaud, J. Bernard, *Chem. Commun*. 2015, 51, 13193.
34. K. Turcheniuk, C.-H. Hage, J. Spadavecchia, A. Y. Serrano, I. Larroulet, A. Pesquera, A. Zurutuza, M. G. Pisfil, L. Heliot, J. Bouckaert, R. Boukherroub, S. Szunerits, *J. Mater. Chem. B* 2015, 3, 375–386.
35. H. Vu-Quang, M. Muthiah, Y.-K. Kim, C.-S. Cho, R. Namgung, W. J. Kim, J. H. Rhee, S. H. Kang, S. Y. Jun, Y.-J. Choi, Y. T. Jeong, I.-Y. Park, *Carbohydr. Polym*. 2012, 88, 780–788.

DOI: 10.1002/cnma.201500229 – Journal: ChemNanoMa– Post-print